JOURNAL OF SPACECRAFT AND ROCKETS
Vol. 41, No. 4, July–August 2004

Tethered Planetary Capture Maneuvers

Paul Williams,* Chris Blanksby,† and Pavel Trivailo‡
Royal Melbourne Institute of Technology, Melbourne, Victoria 3001, Australia

A new concept for the application of space tethers in planetary exploration and payload transfer is presented. We propose the deployment of a payload on a spinning tether in a hyperbolic orbit to provide it with a sufficient velocity change so that it is captured in an elliptical orbit at the destination planet. This concept of using tethers for planetary capture is investigated by conducting numerical simulations of a simplified tether system. The tether mass required to prevent rupture of the tether is optimized using numerical and iterative techniques for each of the major planets in the solar system. It is demonstrated that significant mass savings can be achieved when compared to the requirements for chemical propulsion. Finally, it is shown that controlling the tether length during the maneuver can be used to correct errors in the system trajectory for both spinning and nonspinning capture cases.

Nomenclature

A = tether cross-sectional area, m^2
a = semimajor axis of orbit, m
e = orbit eccentricity
$\boldsymbol{e}$ = eccentricity vector
F = factor of safety for tether material, 1.5
f = orbit true anomaly of the tether system center of mass, rad
g = gravitational acceleration at Earth sea level, 9.81 m/s^2
I_{sp} = specific impulse of chemical propellant, s
i = orbit inclination, rad
J = performance index in optimal control problem
k_1 = nondimensional length control gain
k_2 = nondimensional length rate control gain
L = total desired deployed tether length, m
l = tether length, m
$\boldsymbol{l}$ = unit vector directed along tether-line toward payload, m
m = total system mass ($m_1 + m_2 + m_t$), kg
m_t = tether mass, kg
m_1 = mass of the main spacecraft, kg
m_2 = mass of the payload, kg
m^* = reduced system mass ($[m_1 + m_t/2][m_2 + m_t/2]/m - m_t/6$), kg
R = orbit radius to the center of mass, m
$\boldsymbol{R}_x$ = inertial position vector to element of tether, m
r_p = periapsis radius of approach hyperbolic orbit, m
r_1 = distance to main spacecraft from tether system center of mass, m
r_2 = distance to payload from tether system center of mass, m
T = tether control tension, N
T_G = gravity-gradient torque on dumbbell system, Nm
u = nondimensional control tension ($T/[m_1\{m_2 + m_t\}\dot{f}^2 L/m]$)
$\boldsymbol{V}_x$ = inertial velocity vector of element of tether, m/s
V_∞ = hyperbolic approach velocity, m/s
$\mathcal{E}$ = specific orbital energy, m^2/s^2
θ = in-plane tether libration angle, rad
λ = nondimensional tether length (l/L)
μ = gravitational constant of central planet, m^3/s^2
ρ = tether mass density, kg/m^3
σ_{ut} = ultimate tensile strength of tether material, N/m^2
ϕ = out-of-plane tether libration angle, rad

Superscripts

$\cdot$ = differentiation with respect to time, d( )/dt
$'$ = differentiation with respect to orbit true anomaly, d( )/df

Introduction

SEVERAL proposed applications of tethers in space, particularly in the area of transportation, have generated a lot of interest in the space community.[1–5] Some exciting applications include the use of tethers for aerobraking[6] and injection of payloads into higher orbits,[7–9] including escape orbits.[10–12] The most promising proposed applications involve momentum-exchange techniques. In particular, spinning tether systems in elliptical orbits can be used to transfer sufficient momentum to a payload to allow it to escape Earth orbit and travel to destinations such as the moon and even Mars.

Interplanetary applications of tethers have been considered by a number of authors. Mars missions have received particular focus because of the promise of future human exploration. Lorenzini et al.[13] considered deploying a small tethered probe into the lower Martian atmosphere for dust collection. Optimal configurations for this scenario were later considered by Pasca and Lorenzini.[14,15] Aerocapture maneuvers using tethers were considered by Longuski et al.,[6] and optimal mass configurations are found using mass maps by Tragesser et al.[16] Biswell and Puig-Suari[17] considered controlling the dynamics during aerocapture by using a lifting surface on the probe. Jokic et al.[18] considered a similar scenario, but also investigated the advantages gained by separating the probe and main spacecraft from the tether at an appropriate moment, as well as by varying the tether length.

This paper develops a concept for the use of momentum transfer tethers in interplanetary spaceflight. The heart of the concept, first mentioned by Longuski et al.,[6] is the deployment of a payload via a tether from a spacecraft while on a hyperbolic flyby of a target planet. If the system is made to spin about the mass center, then the angular momentum imparted to the payload, if severed from the tether, can be sufficient to allow it to be captured into an elliptical orbit about the target planet. The maneuver, illustrated in Fig. 1, can be separated into three stages for clarity: 1) the payload is deployed via a tether in a hyperbolic approach orbit and made to spin in the positive direction indicated in Fig. 1, 2) the payload is released from the tether at an appropriately timed moment so that it is captured into an elliptical orbit, and 3) the main spacecraft gains an additional boost and is

Received 6 March 2003; revision received 2 July 2003; accepted for publication 3 July 2003.

*Graduate Student, Department of Aerospace Engineering, G.P.O. Box 2476V; tethers@hotmail.com. Student Member AIAA.
†Senior Research Fellow, Department of Aerospace Engineering, G.P.O. Box 2476V; chris.blanksby@rmit.edu.au.
‡Professor, Department of Aerospace Engineering, G.P.O. Box 2476V; trivailo@rmit.edu.au.

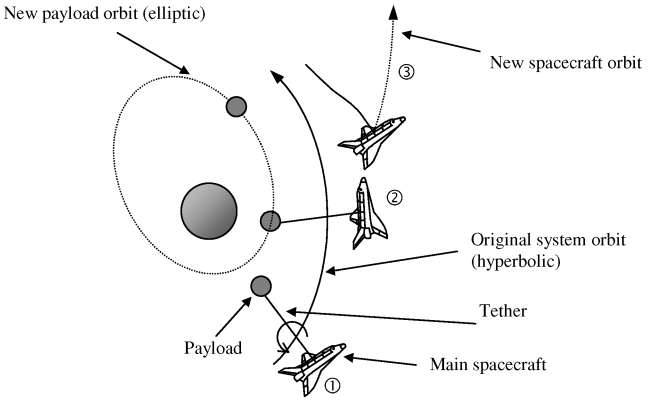

Fig. 1 Tethered planetary capture concept.

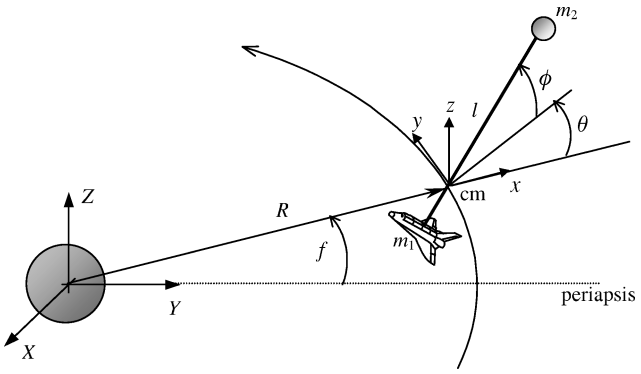

Fig. 2 Simplified representation of tethered dumbbell system.

sent on a new escape trajectory. In this paper we will refer to the proposed maneuver as "tethered planetary capture." Although the basic concept just outlined is simple, the timing of payload release, system configuration, and initial conditions are not straightforward.

The purpose of this paper is to establish the feasibility of using tethers for planetary capture. In this paper a simplified mathematical model of the tethered system is given, and the basic physics of the maneuver are analyzed. Next, a procedure is presented for determining the required tether mass based on the actual physics of the system. The required tether mass is optimized for each of the major planets in the solar system, and the results are compared to the requirements for chemical propulsion. Finally, a method for controlling the maneuver by varying the tether length is investigated.

Mathematical Model

Equations of Motion

In general, tether dynamics are very complex. A flexible tether undergoes a complicated set of coupled vibrations. These can be separated into longitudinal, lateral, and rigid-body modes.[19] All three of these vibratory modes are coupled because of the influence of the gravity-gradient and system nonlinearities. Whereas a detailed study of tether dynamics must inevitably account for the entire range of vibrations, the initial feasibility of a concept can be established/rejected using only a simplified model. In this study a model of the tether dynamics that neglects tether flexibility is adopted. Such models are often used in preliminary tether analyses because of their simplified mathematical representations and computational efficiency.[20]

The major assumptions employed in the derivation of the mathematical model are as follows:

1) The tether is rigid and inextensible but can vary in length in a controlled manner.

2) The only external force acting on the tether system is the Newtonian gravity force from the target planet; aerodynamic drag, solar pressure forces, and the gravity from the sun and other planets are considered negligible.

3) The end masses are considered to be point masses.

4) The tether is uniform in mass.

5) The tether is deployed/retracted from one end mass only.

A representation of the model, as well as the generalized coordinates used to describe the motion, is shown in Fig. 2. The Lagrangian for the system is given by

$$\mathcal{L} = \tfrac{1}{2}[m_1(m_2+m_t)/m]\dot{l}^2 + \tfrac{1}{2}m^*l^2[\dot{\phi}^2 + (\dot{\theta}+\dot{f})^2\cos^2\phi] + \tfrac{1}{2}m(\dot{R}^2 + R^2\dot{f}^2) + \mu m/R - (\mu m^* l^2/2R^3)(1 - 3\cos^2\theta\cos^2\phi) \quad (1)$$

By utilizing Lagrange's equations, the equations of motion of the system can be shown to be

$$\ddot{R} = R\dot{f}^2 - \frac{\mu}{R^2} + \frac{3\mu\Phi_1 l^2}{2R^4}(1 - 3\cos^2\theta\cos^2\phi) \quad (2)$$

$$\ddot{f} = -2\frac{\dot{R}}{R}\dot{f} + \frac{3\mu\Phi_1 l^2}{R^5}\sin\theta\cos\theta\cos^2\phi \quad (3)$$

$$\ddot{\theta} = 2(\dot{\theta}+\dot{f})\left[\dot{\phi}\tan\phi - \Phi_2\frac{\dot{l}}{l}\right] + 2\frac{\dot{R}}{R}\dot{f} - \frac{3\mu}{R^3}\sin\theta\cos\theta\left[1 + \frac{\Phi_1 l^2}{R^2}\cos^2\phi\right] \quad (4)$$

$$\ddot{\phi} = -2\Phi_2\frac{\dot{l}}{l}\dot{\phi} - \left[(\dot{\theta}+\dot{f})^2 + \frac{3\mu}{R^3}\cos^2\theta\right]\sin\phi\cos\phi \quad (5)$$

$$\ddot{l} = -\Phi_3\frac{\dot{l}^2}{l} + \Phi_4 l\left[\dot{\phi}^2 + (\dot{\theta}+\dot{f})^2\cos^2\phi + \frac{\mu}{R^3}(3\cos^2\theta\cos^2\phi - 1)\right] - \frac{T}{m_1(m_2+m_t)/m} \quad (6)$$

where the nondimensional mass parameters have been defined as

$$\Phi_1 = \frac{m^*}{m} \quad (7)$$

$$\Phi_2 = \frac{m_1(m_2+m_t/2)}{mm^*} \quad (8)$$

$$\Phi_3 = \frac{(2m_1-m)(m_t/2)}{m_1(m_2+m_t)} \quad (9)$$

$$\Phi_4 = \frac{m_2+m_t/2}{m_2+m_t} \quad (10)$$

where $m = m_1 + m_2 + m_t$ is the total system mass. Because the orbital time on a hyperbolic orbit is relatively short, it can be assumed that the center of mass remains in an unperturbed Keplerian hyperbolic orbit. Numerical simulations of Eqs. (2–6) show that this is reasonable largely because the orbital perturbations in Eqs. (2) and (3) are proportional to R^{-4} and R^{-5}, respectively. In the case of a Keplerian orbit, the generalized coordinates R and f are known through astrodynamics as

$$R = a(1-e^2)/\kappa \quad (11)$$

$$\dot{f} = \sqrt{[\mu/a^3(1-e^2)^3]}\kappa^2 \quad (12)$$

where $\kappa = 1 + e\cos f$. The convention $a < 0$ is employed in this paper for hyperbolic orbits ($e > 1$). With these modifications and taking the independent variable to be the orbit true anomaly, the nondimensional equations of motion are

$$\theta'' = 2(\theta'+1)[e\sin f/\kappa + \phi'\tan\phi - \Phi_2(l'/l)] - (3/\kappa)\sin\theta\cos\theta \quad (13)$$

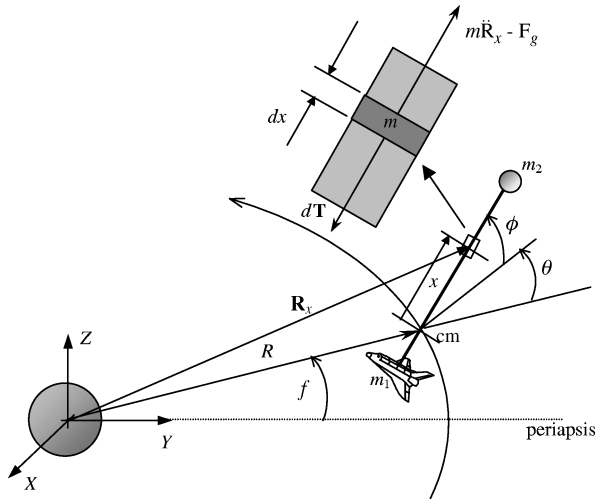

Fig. 3 Elemental tension force on small tether element.

$$\phi'' = (2e\sin f/\kappa)\phi' - 2\Phi_2(l'/l)\phi' - [(\theta'+1)^2 + (3/\kappa)\cos^2\theta]\sin\phi\cos\phi \tag{14}$$

$$l'' = (2e\sin f/\kappa)l' - \Phi_3(l'^2/l) + \Phi_4 l[\phi'^2 + (\theta'+1)^2\cos^2\phi + (1/\kappa)(3\cos^2\theta\cos^2\phi - 1)] - T\Big/\left[m_1\dot{f}^2(m_2+m_t)/m\right] \tag{15}$$

Numerical Software

The equations of motion are integrated using a variable-step, variable-order integration method coded in FORTRAN[21] and implemented in MATLAB® via mex files. All integrations are carried out with relative and absolute tolerances of $1e{-}9$.

Determination of Orbital Parameters for End Masses

Consider the inertial position vector of a point on the tether x, as shown in Fig. 3. Here x is defined to be measured from the center of mass and positive toward mass m_2. Let the inertial position vector to point x be denoted as $\boldsymbol{R}_x$. The inertial position vector to point x can be written as

$$\boldsymbol{R}_x = \begin{Bmatrix} R\cos f + x\cos\phi\cos(f+\theta) \\ R\sin f + x\cos\phi\sin(f+\theta) \\ x\sin\phi \end{Bmatrix} \tag{16}$$

where $-r_1 \le x \le r_2$. Direct differentiation of the position vector gives the velocity

$$\boldsymbol{V}_x = \begin{Bmatrix} \dot{R}\cos f - R\dot{f}\sin f + \dot{x}\cos\phi\cos(f+\theta) - x\dot{\phi}\sin\phi\cos(f+\theta) - x(\dot{f}+\dot{\theta})\cos\phi\sin(f+\theta) \\ \dot{R}\sin f + R\dot{f}\cos f + \dot{x}\cos\phi\sin(f+\theta) - x\dot{\phi}\sin\phi\sin(f+\theta) + x(\dot{f}+\dot{\theta})\cos\phi\cos(f+\theta) \\ \dot{x}\sin\phi + x\dot{\phi}\cos\phi \end{Bmatrix} \tag{17}$$

If either end mass is released from the tether, it will undergo central force motion with constant energy per unit mass[22]:

$$\mathcal{E} = V_x^2\big/2 - \mu/R_x = -\mu/2a_x \tag{18}$$

Therefore the new semimajor axis a_x of either end mass can be determined as

$$a_x = R_x\big/\left(2 - R_x V_x^2\big/\mu\right) \tag{19}$$

The new orbit eccentricity can be determined by utilizing the eccentricity vector, the magnitude of which is the orbit eccentricity[23]

$$\boldsymbol{e} = (1/\mu)\left(V_x^2 - \mu/R_x\right)\boldsymbol{R}_x - (1/\mu)(\boldsymbol{R}_x\cdot\boldsymbol{V}_x)\boldsymbol{V}_x \tag{20}$$

The eccentricity vector points toward the periapsis of the new orbit. If the inertial position and velocity vectors are used to calculate the eccentricity vector, then the vector will also be in inertial coordinates. Therefore, the orbit inclination i can be determined as follows (assuming an initial equatorial orbit):

$$i = \tan^{-1}\left(e_z\Big/\sqrt{e_x^2 + e_y^2}\right) \tag{21}$$

where e_x, e_y, and e_z are the X, Y, and Z components of the eccentricity vector, respectively.

Tether Mass Requirements

To quantify whether it is advantageous to perform the capture maneuver with tethers rather than by burning chemical propellant, it is necessary to establish the mass of tether required to sustain the high tension forces. As has been noted in the derivation of the equations of motion, the tether is assumed to have a uniform cross section. This considerably simplifies the analysis, but also makes the analysis conservative in its estimation of tether mass because the optimal tether configuration would probably involve some tapering.[11] This will be considered at a later time.

The calculation of tether mass depends strongly on an accurate determination of the maximum tension in the tether. For this purpose it is necessary to calculate the tension based on the dynamical response of the system. Note that the tension that can be calculated from Eq. (15) is the control tension, and not necessarily the maximum tension experienced in the tether. To calculate the maximum tension experienced by the tether, consider the dumbbell system shown in Fig. 3. A small element of the tether is considered at a distance x from the center of mass, measured positively toward m_2, as shown in Fig. 3. Because the tether is assumed to be rigid, a longitudinal force is required to keep the elemental mass $\rho A\,\mathrm{d}x$, attached to the tether (because there is a force difference across its surface caused by centripetal acceleration effects). The tension is at its smallest relative value at the attachment points for the end masses and increases nonlinearly to a maximum at the center of rotation of the system.

The inertial position of the element $\mathrm{d}x$ is given by Eq. (16). The differential tension can be found by solving Newton's second law for the unknown force

$$\mathrm{d}\boldsymbol{T} = m\ddot{\boldsymbol{R}}_x - \boldsymbol{F}_g \tag{22}$$

Because this force is assumed to act solely along the tether longitudinal direction, its scalar magnitude and sign can be determined by taking the following dot product:

$$\mathrm{d}\boldsymbol{T}\cdot\boldsymbol{l} = m\ddot{\boldsymbol{R}}_x\cdot\boldsymbol{l} - \boldsymbol{F}_g\cdot\boldsymbol{l} \tag{23}$$

where $\boldsymbol{l}$ is a unit vector directed from mass 1 to mass 2 given by

$$\boldsymbol{l} = \begin{Bmatrix} \cos\phi\cos(f+\theta) \\ \cos\phi\sin(f+\theta) \\ \sin\phi \end{Bmatrix} \tag{24}$$

The gravity force on element $\mathrm{d}x$ can be written as

$$\boldsymbol{F}_g = -\frac{\mu\rho A\,\mathrm{d}x}{|\boldsymbol{R}_x|^3}\boldsymbol{R}_x \tag{25}$$

Substitution of Eqs. (16), (24), and (25) into Eq. (23) and simplifying gives a differential tension of

$$\mathrm{d}T = \rho A\,\mathrm{d}x\left[\frac{\mu(R\cos\theta\cos\phi + x)}{(R^2 + x^2 + 2Rx\cos\phi\cos\theta)^{\frac{3}{2}}} - \frac{\mu}{R^2}\cos\phi\cos\theta - x(\dot{f}+\dot{\theta})^2\cos^2\phi - x\dot{\phi}^2\right] \tag{26}$$

The maximum tension occurs for $\mathrm{d}T = 0$, which occurs when $x = 0$, that is, the center of mass. Hence the maximum tension in the tether can be evaluated by integrating from the tether tip to the center of mass:

$$T_{\max} = T_1 + \int_{x=-r_1}^{x=0} \mathrm{d}T \tag{27}$$

where T_1 is the tension evaluated at mass 1, calculated from Eq. (23) by letting $m = m_1$,

$$T_1 = m_1\left\{r_1[\dot{\phi}^2 + (\dot{f}+\dot{\theta})^2\cos^2\phi] - (\mu/R^2)\cos\phi\cos\theta + \mu(R\cos\phi\cos\theta - r_1)\Big/R_1^3\right\} \tag{28}$$

Evaluation of Eq. (27) gives

$$T_{\max} = r_1[m_1 + \rho A(r_1/2)][\dot{\phi}^2 + (\dot{f}+\dot{\theta})^2\cos^2\phi] - (\mu/R)\{(m_1/R)\cos\phi\cos\theta + \rho A[1 + (r_1/R)\cos\phi\cos\theta]\} + (\mu/R_1)\left[\rho A + m_1(R\cos\phi\cos\theta - r_1)\Big/R_1^2\right] \tag{29}$$

where $R_1 = \sqrt{(R^2 + r_1^2 - 2Rr_1\cos\phi\cos\theta)}$. The required tether mass to sustain the maximum tension force during a maneuver is calculated by determining the tether cross-sectional area as follows:

$$A = \left.\frac{FT_{\max}}{\sigma_{\mathrm{ut}}}\right|_{\max} \tag{30}$$

The tether mass is determined simply from

$$m_t = \rho AL \tag{31}$$

To evaluate Eq. (29), the tether cross-sectional area must be known. Therefore an iterative procedure must be employed: a tether cross-sectional area is assumed, the simulation is performed, and the cross-sectional area is updated based on the maximum tension experienced during the maneuver; the process continues until the cross-sectional area converges to within a prescribed tolerance ($1e{-}7$ is the tolerance used in this paper).

Dynamics of Tethers in Eccentric Orbits

When the tether system moves in a noncircular orbit, the equations of motion are nonautonomous and exhibit forcing terms as a result of the nonuniform variation in orbit angular velocity.[20] These forcing terms cause the tether to librate about the local vertical. The librations become chaotic at orbit eccentricities of about 0.31 (Ref. 24), which coincides with the eccentricity required to cause an initially radially aligned tether at periapsis to start tumbling. The tendency for the tethered system to tumble increases with orbit eccentricity. This tendency can be exploited beneficially in momentum transfer applications.[25] The mechanism behind the tumbling can be identified as the result of the gravity-gradient torque acting on the system. When the tether is in free planar motion about a planet, it experiences a gravity-gradient torque given approximately as[26]

$$T_G = -(3\mu/2R^3)m^*l^2\sin 2\theta \tag{32}$$

Substitution of Eq. (11) into Eq. (32) yields

$$T_G = -\frac{3\mu(1+e\cos f)^3}{2a^3(1-e^2)^3}m^*l^2\sin 2\theta \tag{33}$$

As can be seen from Eq. (33), the gravity-gradient torque for $e \neq 0$ varies with the orbit true anomaly f and is a maximum at periapsis ($f = 0$). The magnitude is maximum with eccentricities close to 1 and at libration angles of $\theta = \pi/4 \pm n\pi/2, n = 1, 2, 3\ldots$. Therefore, it is more likely that tumbling will be initiated in orbits that are near parabolic ($e = 1$) and in the vicinity of the orbit periapsis.

Consider the special case of in-plane motion and a fixed length tether. The equation governing the in-plane libration is, from Eq. (13),

$$\theta'' - 2\theta'(e\sin f/\kappa) + (3/\kappa)\sin\theta\cos\theta = 2(e\sin f/\kappa) \tag{34}$$

Equation (34) shows that the damping of the in-plane librations (second term on left-hand side) is in resonance with the centrifugal forcing term on the right-hand side. This is because of the nonuniform variation in angular velocity of the orbit. It can be seen that the effect of this torque is to cause the tether to be rotationally accelerated against the orbit on approach (f negative) with a subsequent change of direction as it moves away from periapsis (f positive). Because the "damping" is identical in magnitude and sign to the rotational acceleration, it is evident that the damping is positive on approach and negative after periapsis. This tends to suggest that the tether is much more likely to begin tumbling after passing through periapsis, rather than on approach, because the system should be unstable. This reasoning has been verified through numerical simulations of the dynamics of the tethered system in hyperbolic orbits. Figure 4a shows plots of the libration angle vs true anomaly for

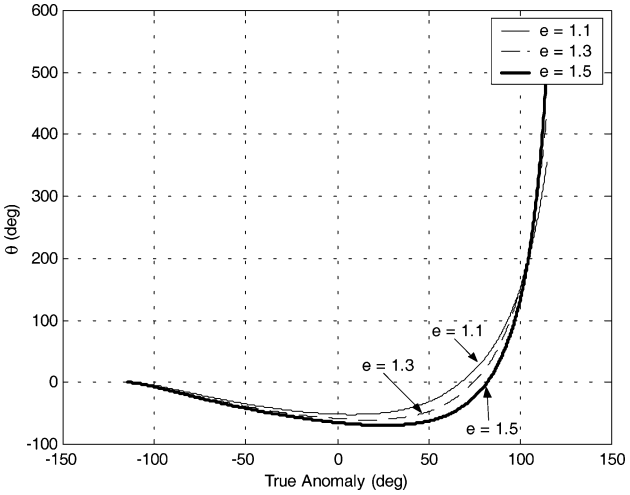

Fig. 4a In-plane libration of tethered system in hyperbolic orbit.

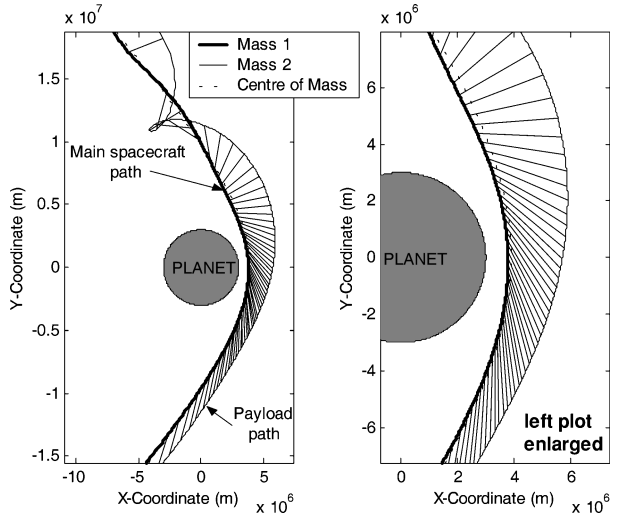

Fig. 4b Snapshots of tether orientation during hyperbolic orbit ($e = 1.5$; tether enlarged).

various orbit eccentricities. Initial conditions are selected for hyperbolic orbits with initial true anomalies to ensure the system is under the central planet's sphere of influence ($-2.0 \leq f \leq 2.0$). The initial libration angle and rate are set to be zero.

Figure 4a can be interpreted as showing that the tether has a tendency to swing "negatively" for negative true anomalies and has a dramatic change at, or slightly following, the passage through periapsis. For eccentricities closer to 1, the change from negative to positive swing rate occurs closer to periapsis. This is in agreement with the preceding discussion. It is also evident that the tether spin rate increases with orbit eccentricity after the passage through periapsis. Figure 4b better represents what actually happens to the system during the hyperbolic orbit. Note that the tether has been dramatically enlarged and that the actual sizes of the planet and tether are fictitious. Figure 4b shows that the tether is barely rotating as it approaches the planet. This is because of the gravity-gradient torque being very weak in the initial stages of the hyperbolic orbit. The apparent change in libration angle in Fig. 4a during this time is actually a result of the change of the radius vector to the center of mass, that is, the nonuniform nature of the variation of the local vertical, rather than any actual inertial rotation of the tether. This, however, abruptly changes at periapsis. The gravity-gradient torque is maximum at this point, and it is evident that the tether commences rotation.

The natural ability for the tether system to commence rotation at or slightly following the passage through periapsis can be utilized effectively in momentum transfer applications. If the system is deployed with the right set of initial conditions, then it is conceivable that the magnitude of the tether spin rate can be controlled so as to produce a desired delta-v at the tether tip. If the spin rate is adjusted in accordance with the system configuration (tether length, system mass ratio, etc.), then the delta-v might be sufficient to cause the payload to be captured into an elliptical orbit. The objective of the following section is to establish the system parameters that are required to give a sufficient delta-v to result in planetary capture.

Optimal Tether Configurations for Planetary Capture

Interplanetary Arrival Conditions

For approximate initial estimates of a representative interplanetary hyperbolic orbit at the destination planet, the patched conic approximation can be used. For simplicity, the arrival conditions are taken from Ref. 6, which contains the arrival velocities at the destination planet for a Hohmann transfer from an initial 200-km low Earth orbit (LEO).

The hyperbolic orbit eccentricity can be calculated from[27]

$$e = r_p v_\infty^2 \big/ \mu + 1 \tag{35}$$

The Δv and mass of propellant required to perform the same maneuver without the tether can be calculated from[6]

$$\Delta v = \sqrt{2\mu/r_p + v_\infty^2} - \sqrt{2\mu/r_p} \tag{36}$$

$$m_{\text{prop}} = m_2(e^{\Delta v/I_{\text{sp}}g} - 1) \tag{37}$$

where I_{sp} is assumed to be 300 s.

The main parameters of the tether system configuration considered throughout this paper are given in Table 1. The planetary arrival conditions and propellant requirements are given in Table 2. These values can be used to make comparisons with the tether mass required to perform the same maneuver.

Numerical Optimization Procedure and Results

The mathematical problem for the minimum mass maneuver can be written as follows:

Determine

$$\min[m_t(\theta_0, \dot{\theta}_0, L, d)]$$

Subject to

$$\min T > 0, \qquad \min e_2 < 0.995, \qquad \max T < (\sigma_{ut}/F)A \tag{38}$$

Table 1 Common system parameters

System parameter	Value
Main spacecraft mass, m_1	8000 kg
Payload mass, m_2	800 kg
Tether ultimate tensile strength, σ_{ut}	4 GPa
Tether mass density, ρ	970 kg/m^3
Factor of safety, F	1.5
Initial true anomaly, f_0	30 deg $-\cos^{-1}(-1/e)$ deg

Table 2 Planetary arrival conditions and chemical propellant requirements for capture of 800-kg payload

Planet	μ, m^3/s^2	V_∞, km/s	r_p, km	e	Δv, km/s	m_{prop}, kg
Venus	$3.25(10)^{14}$	2.71	6,550	1.148	0.362	104.7
Earth	$3.99(10)^{14}$	2.97	6,878	1.152	0.402	117.1
Mars	$4.28(10)^{13}$	2.65	3,898	1.640	0.697	213.9
Jupiter	$1.27(10)^{17}$	5.64	72,300	1.018	0.268	76.2
Saturn	$3.79(10)^{16}$	5.44	61,300	1.048	0.418	122.2
Uranus	$5.80(10)^{15}$	4.66	27,400	1.103	0.521	155.0
Neptune	$6.85(10)^{15}$	4.05	26,000	1.062	0.355	102.4

Table 3 Optimum tether masses for interplanetary capture with 100-km-long tether

Planet	θ_0, deg	$\dot{\theta}_0$, deg/s	d, mm	m_t, kg	%, mass saving
Venus	95	0.16	0.6979	37.1	64.6
Earth	340	0.19	0.7780	46.1	60.6
Mars	25	0.4	1.410	151.5	29.2
Jupiter	150	0.19	0.6594	33.1	56.6
Saturn	25	0.28	0.9394	67.2	45.0
Uranus	225	0.33	1.1195	95.5	38.4
Neptune	190	0.21	0.7331	40.9	60.1

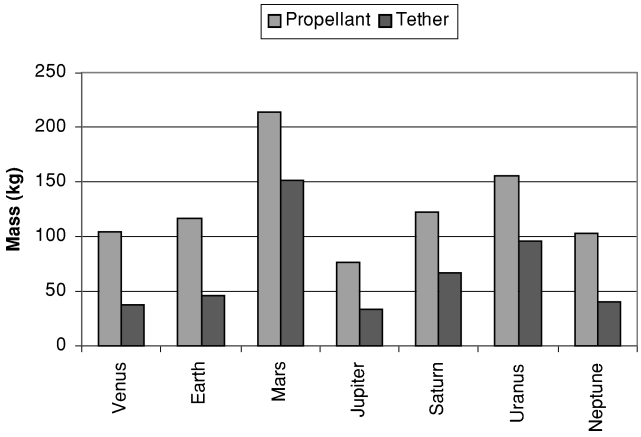

Fig. 5 A 100-km tether mass vs chemical propellant mass requirements for payload capture.

The optimization problem can be reduced by removing the tether diameter as a parameter to be optimized. Instead, the tether diameter can be determined explicitly for each set of initial conditions by an iterative procedure as outlined earlier.

The determination of optimal configurations for planetary capture is nontrivial even though only a few design variables are considered. The tether dynamics are very sensitive to the initial conditions, and therefore optimization routines based on gradient searches are likely to get trapped in local minima. In this paper the global minimum results are obtained by holding the tether length fixed and performing an exhaustive search of the initial conditions. The numerical results, based on a 5-deg and 0.01-deg/s resolution search of the initial conditions, are presented in Table 3 and Fig. 5 for a 100-km-long tether. It is evident that in every case the tether mass requirements are well below those required for capture using chemical propulsion. This result is very promising considering that the mass estimates

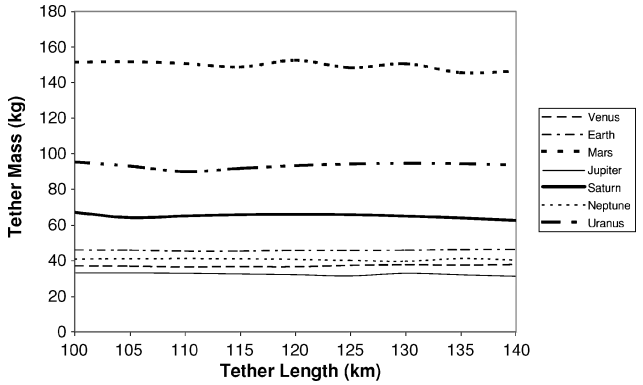

Fig. 6 Optimum tether mass requirements vs tether length.

are based on the actual tether tension experienced by the system and includes a factor of safety on the material. It is found that the greatest absolute mass saving is for capture at Earth, but the greatest relative mass saving is at Venus.

The optimum situation for using tethers to perform the capture maneuver would be when multiple payloads are to be delivered among the solar system. In this situation only one tether system would be required, and the mass savings in propellant for such a mission would be even more significant. It can be noted, however, that the requirements for capture vary considerably among the different planets. The design of the system for multiple capture opportunities among the various planets would need to take into consideration the differing mass requirements and arrival conditions for an "interplanetary tour." This is an area deserving further work.

The procedure used to obtain the results shown in Table 3 was repeated for various tether lengths ranging from 100 to 140 km. The results for this variation are given in Fig. 6. It can be seen in Fig. 6 that the tether mass requirements are relatively insensitive to changes in tether length. Figures 7 and 8 show the variation in required initial conditions with tether length for the optimal mass configurations. Figure 7 demonstrates that the system is very sensitive to initial conditions, particularly the required initial angle. For example, at Mars an increase of 5 km in tether length requires a change of 100 deg in the initial tether angle and a decrease in spin rate of 0.02 deg/s. Similar sensitivities are observed for all planets. Figure 8 shows that an increase in tether length generally leads to a decrease in the required initial spin rate. It might be advantageous to design the system with a longer tether so that the required tether spin rate can be reduced. At Venus, for example, the initial spin rate can be halved from 0.16 to 0.08 deg/s by increasing the tether length from 100 to 135 km. In general, an increase in tether length does not necessarily increase the tether mass requirements, as noted in Fig. 6.

The largest required delta-v are for Mars, Uranus, and Saturn, respectively, which correspond directly to the high required spin-rates for those planets shown in Fig. 8. However, the lower required delta-v for the other planets do not correspond directly to the required initial spin rate. This is because the required initial spin rate for the optimal mass configuration is a complicated function of the required delta-v for the payload, orbit eccentricity, planetary mass, and orbital altitude of the tether system above the planet. Hence it is not easy to predict or explain the required initial conditions.

Example Simulation Results: Capture at Venus

The mass contour maps used for the determination of the optimal configuration more clearly illustrate the sensitivity of the system to initial conditions. These maps are similar to those used by Tragesser et al.[16] As an example, a mass contour map for Venus is given in Fig. 9 with the global minimum mass indicated. Figure 9 shows that the required mass has multiple local minima and that the region containing the global minimum is bounded on all sides by the capture constraint. The dynamics of the optimal point are presented in Figs. 10 and 11. Figure 10a gives the variation in instantaneous orbital eccentricity of the end masses if they were to be severed from the tether. This shows that the change in orbit eccentricity

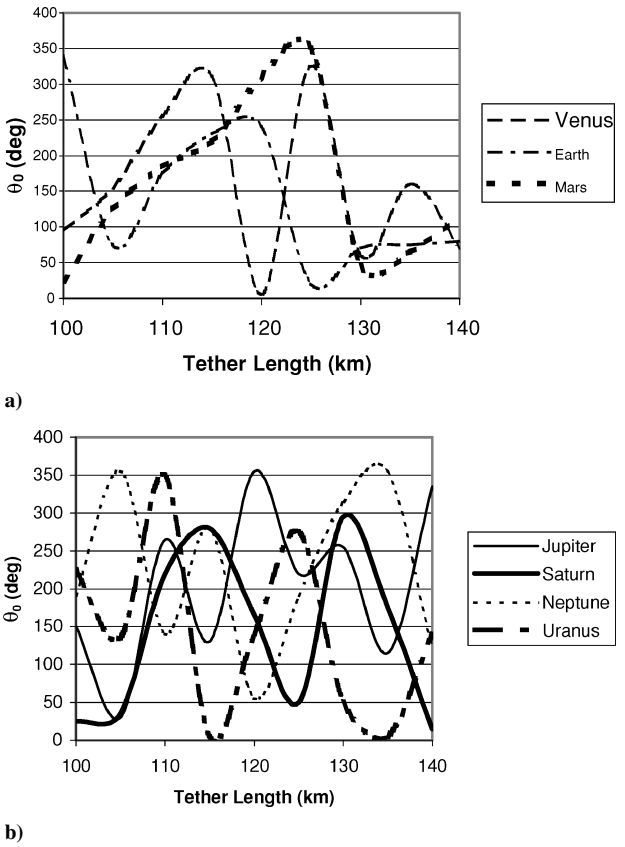

Fig. 7 Variation of optimal initial angle with tether length (top to bottom): a) inner planets and b) outer planets.

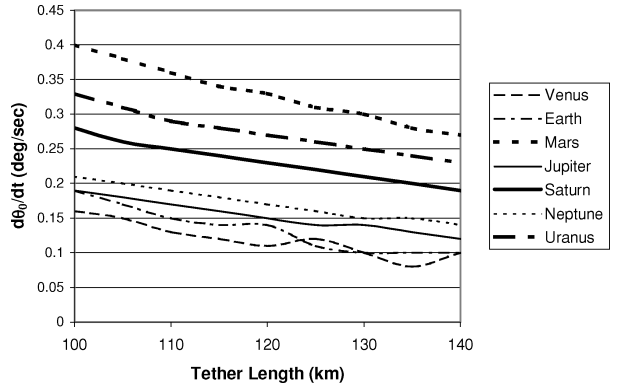

Fig. 8 Variation of optimal initial angular rate with tether length.

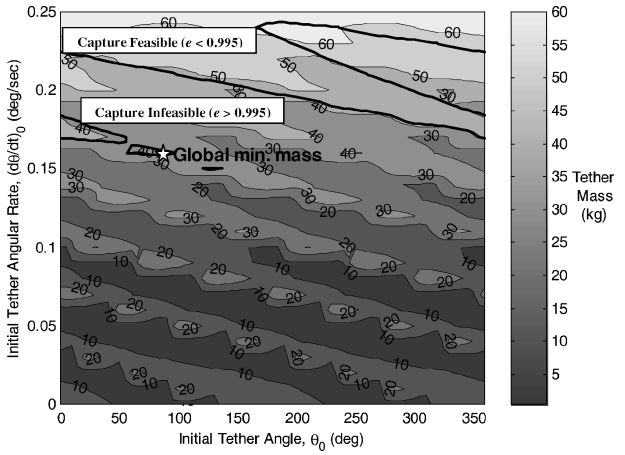

Fig. 9 Tether mass contours for payload capture at venus with 100-km tether.

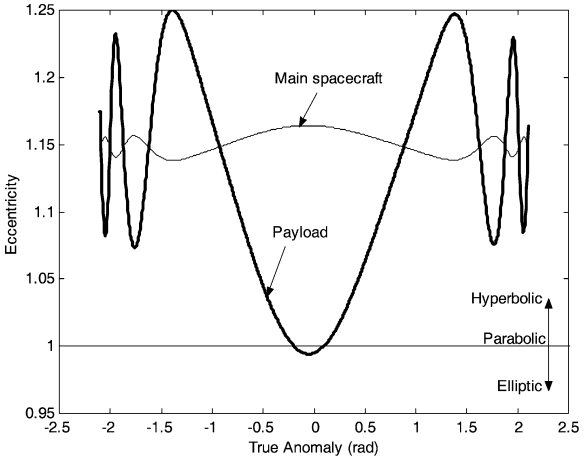

Fig. 10a Orbit eccentricities for end masses during optimum mass maneuver at Venus.

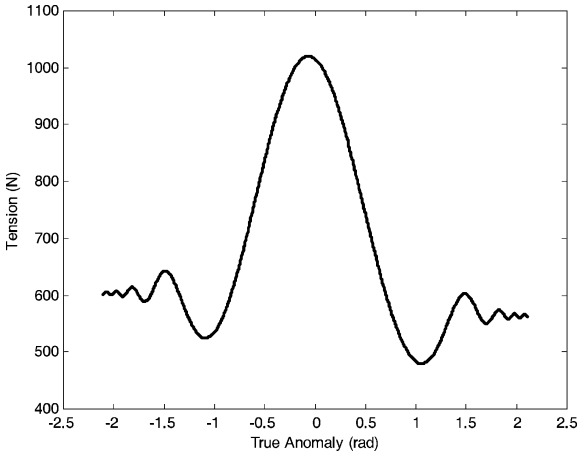

Fig. 10b Tether tension variation during optimum mass maneuver at Venus.

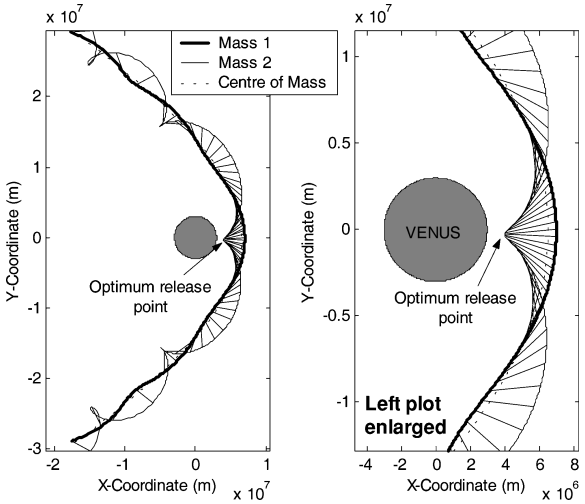

Fig. 11 Tether orientation during optimum mass maneuver at Venus (tether enlarged).

for the payload is more significant in the region of periapsis, with variations between 1.25 and 0.995. Figure 10b gives the maximum tension variation during the maneuver, which averages about 700 N and peaks at just over 1000 N. Figure 11 shows the orientation of the system with respect to the planet in inertial space. It can be seen from Figs. 10a and 11 that the optimal maneuver is nearly symmetric about the orbit periapsis, with payload release occuring during its closest approach to the planet. The effect of the conservation

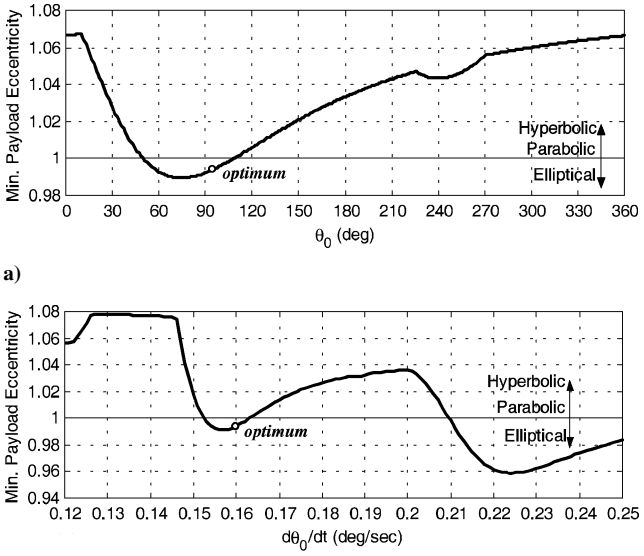

Fig. 12 Variation of minimum achievable eccentricity at Venus with (top to bottom): a) initial angle ($\dot{\theta}_0 = 0.16$ deg/s) and b) initial angular rate ($\theta_0 = 95$ deg).

of momentum is apparent in Fig. 10a, which illustrates the inverse relationship between the instantaneous orbital eccentricities of the end masses. At the optimal release position the tether is aligned along the local vertical, which gives the largest delta-v of the end masses relative to the system center of mass. The main spacecraft can be seen to be given its greatest orbital boost at this point. The large difference between the change in orbital eccentricity for the end masses is caused by the significant difference in mass between the payload and the main spacecraft (1:10).

It is well known that planetary flyby can be utilized in a gravity assist maneuver to produce changes in velocity for a spacecraft. Planetary capture offers the possibility of producing an additional velocity boost. This feature of the proposed technique can be termed momentum-enhanced gravity assist and requires further research to fully explore its possibilities.

The sensitivity of the optimum maneuver for capture at Venus is given in Fig. 12. Figure 12a shows the variation in minimum achievable eccentricity for the payload for various initial angles with the initial angular rate held fixed. It is evident that there is only a small range of initial angles for which capture is possible ($50 \text{ deg} < \theta_0 < 108$ deg) for the given initial spin rate. This implies that the system must be controlled with some precision to achieve the desired accuracy in the initial conditions. Figure 12b shows the variation in minimum achievable eccentricity for the payload for various initial angular rates with the initial angle held fixed. This plot shows that the maneuver is more sensitive to variations in the initial spin rate than to the initial angle. For example, in the worst possible scenario an error of 0.01 deg/s can result in an undesirable change in final eccentricity of 0.08, whereas it takes a change of approximately 60 deg in the initial angle to cause a similar effect. It is also observed that an increase in initial angular rate does not necessarily lead to improvements in beneficial delta-v for the payload. This can be explained by the effect that the initial angular rate has on the orientation of the tether during passage through periapsis. The maximum achievable delta-v occurs when the tether is aligned with the local vertical during passage through periapsis; hence, the combination of initial angle and angular rate needs to be chosen to ensure that this is true. Figures 11 and 12b illustrate that when the tether is aligned with the local vertical at periapsis the required initial angular rate is at a local minimum for achievable payload eccentricity. A similar local minimum occurs at approximately $\dot{\theta}_0 = 0.225$ deg/s in Fig. 12b, although the mean minimum achievable eccentricity for the payload is lower than the preceding case, as expected because of the higher spin rates.

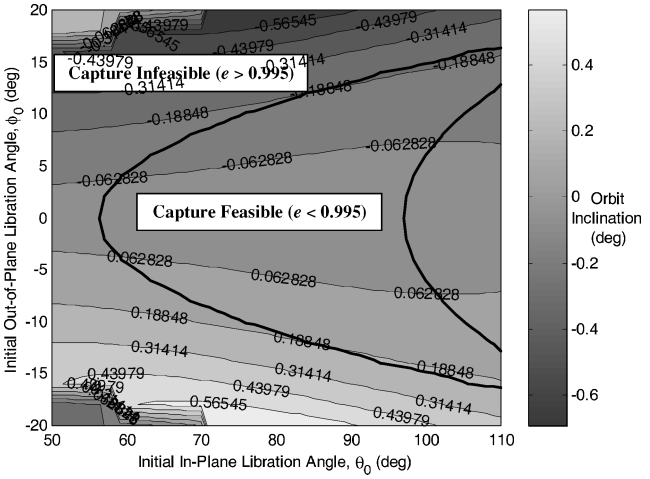

Fig. 13 Contours of change in payload orbit inclination at optimum release point (Venus).

The sensitivity of the maneuver to the initial conditions suggests that it is necessary to provide active control for the system to correct deviations from the planned capture path. Later in this paper we develop a tension control methodology for dealing with the complex nonlinear dynamics.

Out-of-Plane Motion

To achieve planetary capture of a payload by means of a tether requires the generation of a sufficiently large delta-v. Ideally, this delta-v would be produced by the in-plane attitude dynamics of the tether system. However, there might be circumstances where it is advantageous to deliver a payload into an orbit that is inclined relative to the approach orbit. This can again be achieved using tethers, but requires that both in- and out-of-plane motion is present. Out-of-plane motion complicates the dynamics somewhat because the in- and out-of-plane motions are coupled via nonlinear terms, as shown in Eqs. (13) and (14). A systematic variation of the initial libration angles for the optimum capture case at Venus was performed, and the change in orbit inclination of the payload at the optimum release point is plotted in Fig. 13.

Figure 13 illustrates that small perturbations of the system in the out-of-plane direction do not significantly affect the possibility of planetary capture. The effect of such perturbations depends on the selected initial in-plane angle. For example, if $\theta_0 = 60$ deg, then allowances for initial out-of-plane angles of 5 deg are acceptable. However, for the optimal angle of $\theta_0 = 95$ deg allowances of approximately 13 deg are acceptable. Furthermore, only slight changes in orbit inclination appear to be possible (0.18 deg for $\theta_0 = 95$ deg, $\phi_0 = 13$ deg). Figure 14 shows the instantaneous variations in orbit inclination and orbit eccentricity for the end masses during a capture maneuver with initial conditions $(\theta_0, \dot{\theta}_0, \phi_0, \dot{\phi}_0) = (110$ deg, 0.16 deg/s, 10 deg, 0). Figure 14a shows that changes in orbit inclination on the order of 1 deg are possible for this particular case, but these occur well away from periapsis and the optimal payload release point. The physical explanation for this is that the center of mass velocity is much lower for larger absolute true anomalies, and therefore the delta-v in the out-of-plane direction is larger relative to the delta-v at periapsis passage. Hence, although it is generally not possible to achieve significant changes in orbit inclination these results demonstrate that the planetary capture maneuver can be designed to be robust to out-of-plane perturbations.

Control of the Capture Maneuver

The results from the preceding section show that tethered planetary capture offers advantages over the conventional propellant burning maneuver. However, it has also been shown that the maneuver is quite sensitive to the selection of initial conditions. In addition, the ability to have a tether spinning quite rapidly in the early stages of a hyperbolic orbit might be very difficult to achieve. Therefore,

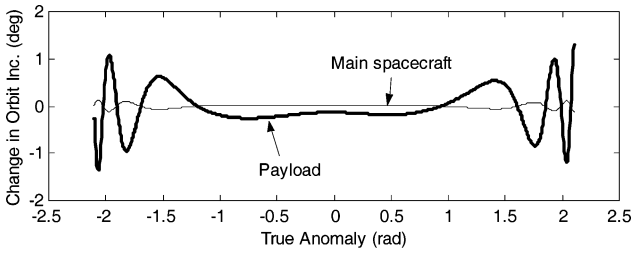

Fig. 14a Change in orbit inclination at Venus with out-of-plane motion.

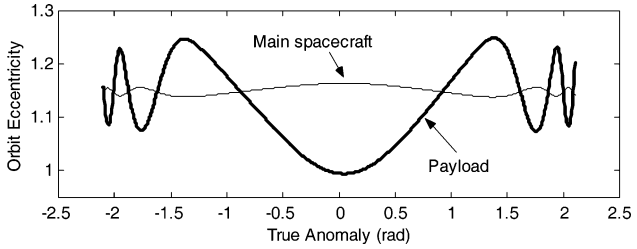

Fig. 14b Orbit eccentricity of end masses at Venus with out-of-plane motion.

the need to be able to actively control the maneuver appears to be of paramount importance. This section examines whether it is possible to control the tether system during the hyperbolic orbit from an initial state where capture is infeasible to a state where capture can be achieved.

In general, the tether attitude dynamics can be controlled by manipulating the tether length. However, such control is limited to cases where the tether tension remains positive. Hence the control is most adequately implemented by adjusting the tether tension at the deployer on the main spacecraft as suggested by Rupp.[28] A control constraint can be introduced that maintains the tether tension above zero. The difficulty of the control problem, as well as the nonlinear nature of the dynamics, means that an innovative method of solution is required.

Formulation of Control Problem

The control problem can be posed in the form of the minimization of a functional, or an optimal control, problem. There are many ways in which such a problem can be set up, but generally it is important to understand the dynamics of the maneuver. In particular, many optimal control problems include a quadratic function of the control input in the performance index. This would be acceptable if the nominal control input were zero. However, in the case of a tether system the tether tension is distinctly nonzero even when the tether length is not being adjusted. Therefore penalizing the tether tension is not a good measure of penalizing the control performance. Because control of the tether is obtained through changes in tether length, the appropriate control input to penalize would be the tether length rate. Therefore the optimal control problem is defined as follows: to obtain the optimal tension input $T(f)$ for $f_0 \le f \le f_f$ that minimizes the performance index

$$J = \max(|\dot{l}|) \tag{39}$$

subject to Eqs. (13) to (15), with initial conditions

$$\begin{Bmatrix} \theta(0) \\ \dot{\theta}(0) \\ \phi(0) \\ \dot{\phi}(0) \\ l(0) \\ \dot{l}(0) \end{Bmatrix} = \begin{Bmatrix} \theta_0 \\ \dot{\theta}_0 \\ \phi_0 \\ \dot{\phi}_0 \\ l_0 \\ \dot{l}_0 \end{Bmatrix} \tag{40}$$

and the constraints

$$\min e_2 - 0.995 \leq 0 \tag{41}$$

$$T(f) > 0 \tag{42}$$

The goal of the optimal control problem is to minimize the maximum length rate experienced by the tether deployer (either reeling in or out) such that capture is achieved at some point during the maneuver. Note that this is not a conventional optimal control problem in that the desired final state (i.e., capture of the payload) is not a straightforward function of the state variables. Therefore it is not convenient to convert the problem from fixed final time to free final time and have the capture of the payload occur at the final time f_f. For this reason the eccentricity for capture is included as an inequality constraint, as in Eq. (41).

Numerical Solution Method

There are many solution methods available for solving optimal control problems. The conventional technique involves employing the calculus of variations and the introduction of costate equations that must be integrated backwards in time.[29] A good review of some numerical solution techniques is given by Betts.[30] Betts classifies solution techniques into direct or indirect methods. Indirect methods solve the problem by tackling the two-point boundary value problem (TPBVP). A number of techniques are available for solving TPBVPs, including shooting,[29] multiple-shooting,[31] gradient,[29] conjugate-gradient,[32] and continuation methods.[33] In these methods the control is defined as a function of the unknown costates, which are iterated upon until a solution is obtained. Shooting methods iterate on the unknown boundary conditions for the costates, whereas gradient methods iterate on the control history itself (as a function of the costates). The ability to handle complicated nonlinear constraints is very difficult, if not impossible using these methods. In contrast, direct methods do not rely upon the costate equations to solve the problem. Direct methods discretize the state and/or control variables and adjust them directly so as to minimize the objective function. In this sense direct methods become nonlinear programming problems. Methods that directly vary the states and control input at a finite number of mesh points are referred to as direct transcription or direct collocation methods.[34,35] Hull[36] has categorized the available methods by the numerical integration technique.

To avoid the inevitable discretization error in traditional collocation techniques, we deal only with explicit integration and parameterization of the control input. The conventional technique[36] for solving the control optimization problem involves parameterizing the control input into a series of nodes. Then, depending on the level of computation available, the control input can be kept fixed between nodes or interpolated. Interpolation can be either linear or cubic, or even higher order, but the higher the order of interpolation the more wavy the resulting control trajectory becomes, and this can affect the stability of the numerical integration. This method is not particularly desirable because a high level of fidelity for the control input is required to maintain control of the tether when tension control is used. The reason for this is that there is always a nominal nonzero tether tension for a fixed length tether, which is a complicated function of the tether states (for example, see Fig. 10b). To overcome this difficulty, the nondimensional tension control input u can be formulated as follows:

$$u = u_0 + k_1(\lambda - \lambda_c) + k_2\lambda' \tag{43}$$

where u_0 is the nondimensional control input required for zero length acceleration for $k_1 = k_2 = 0$.

When the tension control is considered as in Eq. (43), the control input to the numerical optimization routine becomes the commanded length λ_c. In this regard, a very coarse mesh can be utilized to solve for the variation in commanded length because the actual control input includes terms highly dependent on the actual tether dynamics. This is superior to the conventional method of interpolating the control input directly because the order to the nonlinear programming problem can be reduced significantly while retaining high accuracy in the control input.

The commanded length is optimized by selecting n nodal points and using linear interpolation between the nodes. The corresponding nonlinear programming problem is to find the nodal values of the commanded length. In this paper the nonlinear programming problem is solved using a simulated annealing algorithm[37] implemented in MATLAB®. For the current problem formulation it has been found that the simulated annealing approach is superior to gradient-based algorithms because of the sensitivity of the nonlinear constraints. Simulated annealing algorithms cannot explicitly incorporate inequality constraints, which must be included in the cost function via penalty functions. The initial annealing temperature is set as 10,000 K and reduced by a factor of 0.95 each 80 iterations. The tolerance for convergence is set as $1e{-}6$.

Table 4 System parameters for controlled planetary capture simulations

System parameter	Case 1: spinning capture	Case 2: nonspinning capture
Main spacecraft mass	8000 kg	8000 kg
Payload mass	800 kg	800 kg
Nominal tether length	100 km	150 km
Tether line density	0.371 kg/km	0.371 kg/km
Capture eccentricity, e_2	0.995	0.995
Control gains, (k_1, k_2)	(100, 10)	(100, 10)
Control discretization	13	33
$(\theta_0, \theta_0', \phi_0, \phi_0', \lambda_0, \lambda_0')$	(120 deg, 0.16 deg/s, 0, 0, 1, 0)	(180 deg, 0, 0, 0, 1, 0)

Numerical Results for Controlled Planetary Capture

Two controlled capture cases are considered in this paper. The first is capture at Venus with a nominal 100-km-long tether and initial conditions perturbed slightly from optimal. The second is for capture at Venus with an initially nonlibrating tether. The first case is used to demonstrate the possibility of correcting errors in the system trajectory, whereas the second case is used to demonstrate the possibility of planetary capture without the system spinning rapidly on approach. The system parameters used for the numerical simulations are given in Table 4. For capture to be possible for a nonspinning tether, it is necessary to increase the tether length from 100 to 150 km. The minimum achievable eccentricity for a 150-km initially nonspinning tether is 1.0024 ($\theta_0 = 156$ deg). Therefore the case selected will determine whether it is possible to change an infeasible capture scenario to one where planetary capture of the payload can occur through intervention of a control system.

Numerical simulation results for case 1 are shown in Figs. 15 and 16, together with results for simulations where no active control is provided. Figure 15a shows the history of the instantaneous eccentricity of the payload if it were to be released from the tether. This plot shows that without active control the payload does not achieve planetary capture because the instantaneous eccentricity remains above 1, which is consistent with the selection of initial conditions from Fig. 12a. It also demonstrates that by appropriate tether reeling planetary capture of the payload becomes possible just prior to the orbit periapsis. Figure 15b gives the required tension control input, whereas Figs. 16a and 16b give the tether length history and reel rate, respectively. Note that the control input after the payload release point is of no interest in this discussion, and a different control scheme would need to be implemented for postrelease scenarios.[38] Figure 16a shows that a variation in tether length of approximately 5 km is necessary to make capture feasible. Figure 15b shows that an increase in tension of approximately 100 N over the design tension is necessary to implement the control law. Figure 16b shows that a maximum reel rate of about 100 m/s is required to provide active control for this case and that the payload is being reeled in toward the main spacecraft at the optimum release point. This reel rate is somewhat larger than the maximum reel rates provided by current reel mechanisms, but might be achievable in the near future. Finally, it can be noted for Figs. 15 and 16 that the proposed

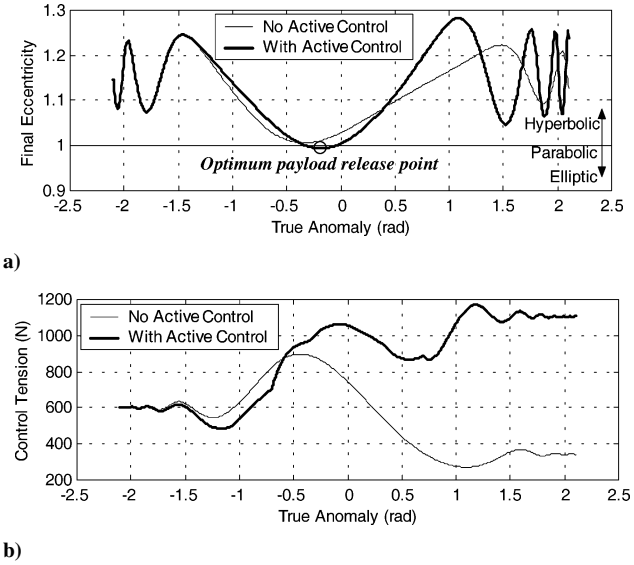

Fig. 15 Controlled capture at Venus with nominal spinning 100-km tether (top to bottom): a) payload eccentricity and b) control tension.

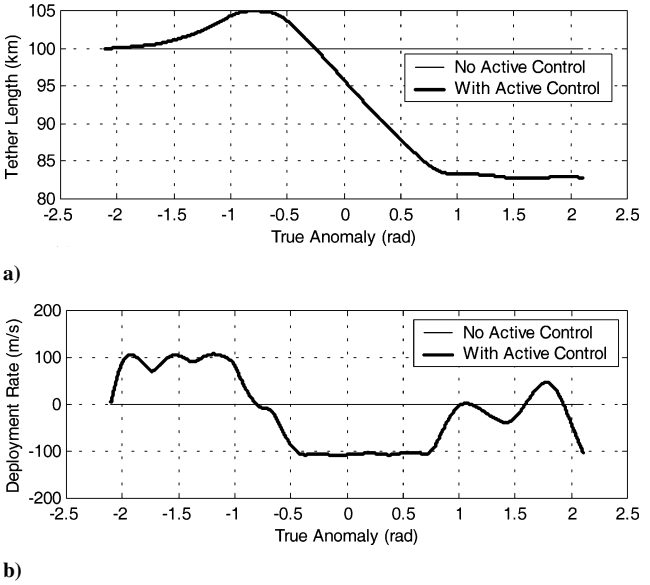

Fig. 16 Controlled capture at Venus with nominal spinning 100-km tether (top to bottom): a) tether length history and b) tether reel rate.

control law gives extremely smooth variations in the system parameters considering that only 13 nodes have been used for the control discretization. This demonstrates the superior nature of the control scheme over the conventional discretization technique for handling difficult nonlinear tether control problems.

Numerical simulation results for case 2 are shown in Figs. 17 and 18, together with results for simulations where no active control is provided. Figure 17a shows that capture is possible using an initially nonspinning tether. It can be noted that the optimum payload release point occurs after orbit periapsis, which is consistent with the results presented earlier. That is, the system commences spinning naturally at periapsis, except in this case tether reeling is utilized to augment the tumbling motion. Figure 18 shows that the reeling requirements are larger than in the preceding case (maximum reel rate 135 m/s), which is consistent with the fact that more intervention is required in this case to achieve capture. The maximum control tension (Fig. 17b) at the optimum payload release point is calculated to be approximately 92% of the design tension. Based on the maximum tether length, the tether mass required for this controlled maneuver is calculated to be 58.5 kg, which is approximately 56% of the propellant mass required for the same maneuver. It can be concluded

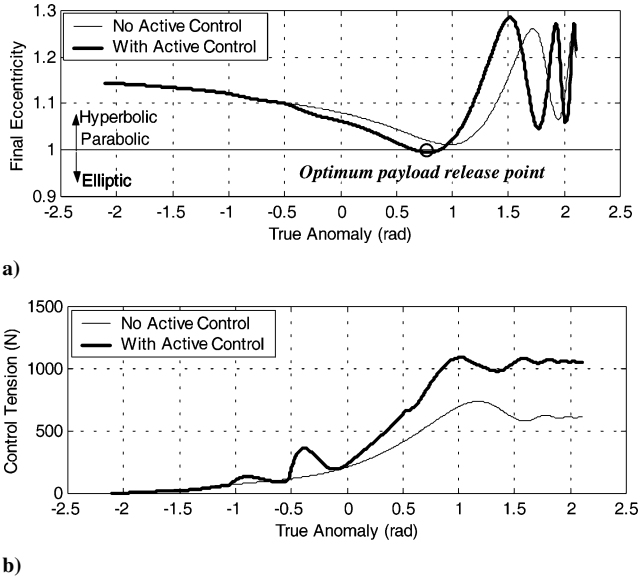

Fig. 17 Controlled capture at Venus with nominal nonspinning 150-km tether (top to bottom): a) payload eccentricity and b) control tension.

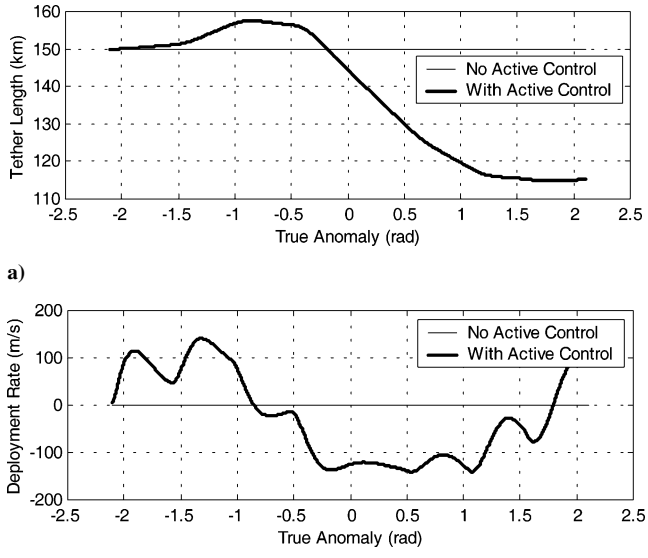

Fig. 18 Controlled capture at Venus with nominal nonspinning 150-km tether (top to bottom): a) tether length history and b) tether reel rate.

for this case that, although active control increases the overall tether mass requirements, it provides for more realistic capture maneuvers without the need for an initially spinning tether.

Conclusions

This paper has presented the concept of using tethers to perform planetary capture maneuvers. The feasibility of the concept has been established by numerically integrating the equations of motion for the system. The major benefit of the concept is that payloads can be captured into elliptical orbits around a target planet with no chemical propulsion while boosting the orbit of the main spacecraft. This has been validated through numerical simulations. It has also been shown that for each of the major planets significantly lower tether mass is required compared to the corresponding chemical propellant requirements. Finally, it has been shown that it is possible to provide active control during the maneuver by varying the tether length in a judicious manner. In particular, it is possible to take the system from a state where capture is infeasible to one where capture can be

achieved. The concept presented in this paper provides a practical alternative to the use of chemical propellant in the future exploration of the solar system. It is evident that further research is required to fully explore the possibilities of the concept proposed in this paper.

References

[1]Cosmo, M. L., and Lorenzini, E. C., *Tethers in Space Handbook*, 2nd ed., Smithsonian Astrophysical Observatory, Cambridge, MA, 1989, Chaps. 2 and 3.

[2]Carroll, J. A., "Tether Applications in Space Transportation," *Acta Astronautica*, Vol. 13, No. 4, 1986, pp. 165–174.

[3]Bekey, I., "Tethers Open New Space Options," *Astronautics and Aeronautics*, Vol. 21, April 1983, pp. 32–40.

[4]Penzo, P., "A Survey of Tether Applications to Planetary Exploration," *Advances in the Astronautical Sciences*, Vol. 62, 1987, pp. 71–87.

[5]Lorenzini, E. C., Cosmo, M., and Kaiser, M., "Tether Transport System Study Summary," *Proceedings of the Tether Technology Interchange Meeting*, edited by J. K. Harrison, NASA CP-1998-206900, 1997, pp. 255–269.

[6]Longuski, J. M., Puig-Suari, J., and Mechalas, J., "Aerobraking Tethers for the Exploration of the Solar System," *Acta Astronautica*, Vol. 35, No. 2/3, 1995, pp. 205–214.

[7]Kumar, K., Kumar, R., and Misra, A. K., "Effects of Deployment Rates and Librations on Tethered Payload Raising," *Journal of Guidance, Control, and Dynamics*, Vol. 15, No. 5, 1992, pp. 1230–1235.

[8]Kyroudis, G. A., and Conway, B. A., "Advantages of Tether Release of Satellites from Elliptic Orbits," *Journal of Guidance, Control, and Dynamics*, Vol. 11, No. 5, 1988, pp. 441–448.

[9]Sorensen, K. F., "Conceptual Design and Analysis of an MXER Tether Boost Station," AIAA Paper 2001-3915, July 2001.

[10]Hoyt, R. P, Forward, R. L., Nordley, G. D., and Uphoff, C. W., "Rapid Interplanetary Tether Transport Systems," International Astronautical Federation, IAF Paper 99-A.5.10, Oct. 1999.

[11]Forward, R., and Nordley, G., "Mars–Earth Rapid Interplanetary Tether Transport System: Initial Feasibility Analysis," *Journal of Propulsion and Power*, Vol. 17, No. 3, 2001, pp. 499–507.

[12]Nordley, G., "Tether-Tossed Mars Mission Examples," AIAA Paper 2001-3375, July 2001.

[13]Lorenzini, E. C., Grossi, M. D., and Cosmo, M., "Low Altitude Tethered Mars Probe," *Acta Astronautica*, Vol. 21, No. 1, 1990, pp. 1–12.

[14]Pasca, M., and Lorenzini, E. C., "Collection of Martian Atmospheric Dust with a Low Altitude Tethered Probe," *Advances in the Astronautical Sciences*, Vol. 75, 1991, pp. 1121–1139.

[15]Pasca, M., and Lorenzini, E. C., "Optimization of a Low Altitude Tethered Probe for Martian Atmospheric Dust Collection," *Journal of the Astronautical Sciences*, Vol. 44, No. 2, 1996, pp. 191–205.

[16]Tragesser, S. G., Longuski, J. M., and Puig-Suari, J., "Global Minimum Mass for Aerobraking Tethers," *Journal of Guidance, Control, and Dynamics*, Vol. 20, No. 6, 1997, pp. 1260–1262.

[17]Biswell, B. L., and Puig-Suari, J., "Analysis of Tether Aerobraking Maneuvers Using a Lifting Probe with Parametric Uncertainties," *Proceedings of the 11th Annual AAS/AIAA Space Flight Mechanics Meeting*, 2001, pp. 1839–1856.

[18]Jokic, M. D., Asokanthan, S. F., Daniel, W. J. T., and Mee, D. J., "Aerogravity Assist Manoeuvring of a Tethered Satellite System," *Proceedings of the AIAA Atmospheric Flight Mechanics Conference and Exhibit*, AIAA, Reston, VA, 2001, pp. 169–178.

[19]Arnold, D. A., "The Behavior of Long Tethers in Space," *Journal of the Astronautical Sciences*, Vol. 35, No. 1, 1987, pp. 3–18.

[20]Beletsky, V. V., and Levin, E. M., "Dynamics of Space Tether Systems," *Advances in the Astronautical Sciences*, Vol. 83, 1993, Chap. 1.

[21]Hindmarsh, A. C., "ODEPACK, A Systematized Collection of ODE Solvers," *Scientific Computing*, edited by R. S. Stepleman, Vol. 1, IMACS Transactions on Scientific Computation, North-Holland, Amsterdam, 1983, pp. 55–64.

[22]Sidi, M. J., *Spacecraft Dynamics and Control*, Cambridge Univ. Press, Cambridge, England, U.K., 1997, p. 15.

[23]Bate, R. R., Mueller, D. D., and White, J. E., *Fundamentals of Astrodynamics*, Dover, New York, 1971, p. 26.

[24]Fujii, H. A., and Ichiki, W., "Nonlinear Dynamics of the Tethered Subsatellite System in the Station Keeping Phase," *Journal of Guidance, Control, and Dynamics*, Vol. 20, No. 2, 1997, pp. 403–406.

[25]Yoshimura, S., "Preliminary Numerical Analysis of the Orbit Transfer Utilising the Tether System Attitude Dynamics," International Astronautical Federation, IAF Paper 01-A.4.09, Oct. 2001.

[26]Koakutsu, H., Nakajima, A., Ota, S., and Nakasuka, S., "Control of a Micro Tether-System for Inducing Rotational Motion on Elliptical Orbit," *Proceedings of the 21st International Symposium on Space Technology and Science*, Vol. 1, 21st ISTS Publications Committee, Omiya, Japan, 1998, pp. 755–762.

[27]Kaplan, M. H., *Modern Spacecraft Dynamics and Control*, Wiley, New York, 1976, p. 93.

[28]Rupp, C. C., "A Tether Tension Control Law for Tethered Subsatellites Deployed Along the Local Vertical," NASA TMX-64963, Sept. 1975.

[29]Kirk, D. E., *Optimal Control Theory: An Introduction*, Prentice–Hall, Upper Saddle River, NJ, 1970, Chap. 6.

[30]Betts, J. T., "Survey of Numerical Methods for Trajectory Optimization," *Journal of Guidance, Control, and Dynamics*, Vol. 21, No. 2, 1998, pp. 193–207.

[31]Morrison, D. D., Riley, J. D., and Zanzanaro, J. F., "Multiple Shooting Method for Two-Point Boundary Value Problems," *Communications of the ACM*, Vol. 5, No. 12, 1962, pp. 613, 614.

[32]Lasdon, L. S., Mitter, S. K., and Waren, A. D., "The Conjugate Gradient Method for Optimal Control Problems," *IEEE Transactions on Automatic Control*, Vol. AC-12, No. 2, 1967, pp. 132–138.

[33]Ohtsuka, T., and Fujii, H., "Stabilized Continuation Method for Solving Optimal Control Problems," *Journal of Guidance, Control, and Dynamics*, Vol. 17, No. 5, 1994, pp. 950–957.

[34]Enright, P. J., and Conway, B. A., "Optimal Finite-Thrust Spacecraft Trajectories Using Collocation and Nonlinear Programming," *Journal of Guidance, Control, and Dynamics*, Vol. 14, No. 5, 1991, pp. 981–985.

[35]Enright, P. J., and Conway, B. A., "Discrete Approximations to Optimal Trajectories Using Direct Transcription and Nonlinear Programming," *Journal of Guidance, Control, and Dynamics*, Vol. 15, No. 4, 1992, pp. 994–1002.

[36]Hull, D. G., "Conversion of Optimal Control Problems into Parameter Optimization Problems," *Journal of Guidance, Control, and Dynamics*, Vol. 20, No. 1, 1997, pp. 57–60.

[37]Press, W. H., Teukolsky, S. A., Vetterling, W. T., and Flannery, B. P., *Numerical Recipes in C++, The Art of Scientific Computing*, 2nd ed., Cambridge Univ. Press, Cambridge, England, U.K., 2002, pp. 448–460.

[38]Nigjeh, B. K., Blanksby, C., and Trivailo, P., "Post-Capture Scenarios for Space Tether Missions," International Astronautical Federation, IAC Paper 02-A.5.03, Aug. 2002.

D. Spencer
Associate Editor